Transport in Porous Media (2022) 143:681–702
https://doi.org/10.1007/s11242-022-01804-5

# A Numerical Investigation on Effective Diffusion in Cement-Based Composites: The Role of Aggregate Shape

**Qingchen Liu[1] · Deheng Wei[1] · Hongzhi Zhang[2] · Chongpu Zhai[4] · Yixiang Gan[1,3]**

Received: 21 November 2021 / Accepted: 18 May 2022 / Published online: 25 June 2022


**Abstract**
Diffusive behaviour is the fundamental mechanism of ionic-induced corrosion in cement–granular composites. Aggregate characteristics, including shape anisotropy, spatial orientation, and size distribution, significantly influence effective diffusivity. However, influences of all such types of aggregate irregularity have rarely been systematically quantified, and most of the representative aggregate shapes in numerical simulations are convex than realistic concave. In this study, we apply the finite element method (FEM) to investigate diffusion behaviour of 2D cement-based composites. Realistic multi-scale aggregate shapes, characterised by fractal dimension ($F_d$) and relative roughness ($R_r$), are generated to highlight the influence of aggregate morphology on the effective diffusivity. The spatial distribution is evaluated by the disorder index. From numerical results, samples with a larger disorder index, indicating a broader throat size distribution, show smaller effective diffusivities. Meanwhile, aggregate shape irregularity causes much smaller effective diffusivities, highlighting the necessity of the realistic concave particle shapes in numerical simulations. Sensitivity studies show $F_d$ and $R_r$ are more related to the effective diffusivity than other single-scale classical shape parameters. At last, a model with only these two shape parameters is proposed to predict effective diffusivity. This work further improves the understanding of the role of aggregate morphology on the effective diffusivity, towards applications in ionic-induced corrosion in two-phase composites.

## Highlights

- Realistic grain shapes in composites are generated using Fourier transformation.
- Effects of aggregate characteristics on the effective diffusivity are investigated.
- $F_d$ and $R_r$ are key geometrical parameters influencing the effective diffusivity.

✉ Deheng Wei
dwei3017@uni.sydney.edu.au

✉ Yixiang Gan
yixiang.gan@sydney.edu.au

Extended author information available on the last page of the article

**Keywords** Effective diffusivity · Cement-based composite · Disorder index · Aggregate morphology

**List of symbols**

| | |
|---|---|
| $N_p$ | Number of points on particle contour |
| $P_i$ | Point on the particle contour |
| $\theta_P$ | Polar angle away from positive $x$-direction |
| $l_i$ | Distance between point $P_i$ and centre of particle contour |
| $n$ | Number of discrete signals |
| $N$ | Total number of discrete signals |
| $X_n, Y_n$ | Discrete signal after Fourier transformation |
| $l_0$ | Average of discrete signals |
| $F_n$ | Normalised amplitude |
| $F_d$ | Fractal dimension |
| $H$ | Hurst coefficient |
| $R_r$ | Relative roughness |
| $c$ | Concentration ($\mathrm{mol/m^3}$) |
| $x$ | Horizontal displacement (m) |
| $dc/dx$ | Concentration gradient ($\mathrm{mol/m^4}$) |
| $J$ | Diffusion flux ($\mathrm{mol/m^2/s}$) |
| $D_{\mathrm{eff}}$ | Effective diffusivity of cement-based composite ($\mathrm{m^2/s}$) |
| $D_{\mathrm{eff,\,u}}, D_{\mathrm{eff,\,u}}, 1$ | Hashin–Shtrikman upper and lower bounds of effective diffusivity $\mathrm{m^2/s}$) |
| $D_c, D_a$ | Diffusion coefficient of the cement paste and aggregates ($\mathrm{m^2/s}$) |
| $D_0$ | Effective diffusivity of cement-based composite with hexagonal packing of circular aggregates ($\mathrm{m^2/s}$) |
| $\frac{D_{\mathrm{eff}}}{D_0}$ | Dimensionless effective diffusivity |
| $I_v$ | Disorder index |
| $N_a$ | Number of aggregates in the cement paste |
| $\phi_k$ | Local solid fraction within the Voronoi cell |
| $\phi$ | Overall solid fraction in the cement paste |
| $\sigma_{\mathrm{rt}}$ | Standard deviation of relative throat size distribution |
| $HS_u$ | Dimensionless Hashin–Shtrikman upper bound |
| $d_{\mathrm{ap}}$ | Apparent diameter of circular aggregates (m) |
| $\gamma$ | Associated parameters controlling apparent diameter |
| $d$ | Original diameter of circular aggregates (m) |
| $EI$ | Elongation of aggregates |
| $\sigma_{\frac{D_{\mathrm{eff}}}{D_0}}$ | Standard deviation of effective diffusivity $\frac{D_{\mathrm{eff}}}{D_0}$ |
| $\sigma_{\mathrm{rt,avg}}$ | Average standard deviation of relative throat size distribution |
| $A_{\mathrm{s}}$ | Projected area of an aggregate particle ($\mathrm{m^2}$) |
| $A_{\mathrm{cir}}$ | Area of the minimum circumscribing circle ($\mathrm{m^2}$) |
| $d_{\mathrm{c}}$ | Diameter of a circle having the same projected area as the particle (m) |
| $d_{\mathrm{cir}}$ | Diameter of the minimum circumscribing circle (m) |
| $r_{\mathrm{cir}}$ | Radius of the minimum circumscribing circle (m) |
| $P_{\mathrm{c}}$ | Perimeter of a circle having the same projected area as the particle (m) |
| $r_{\mathrm{insc}}$ | Radius of the largest inscribed circle in the particle (m) |
| $r_{\mathrm{c}}$ | Radius of the circles that approximate the corners of the particles contour (m) |
| $P_{\mathrm{s}}$ | Perimeter of the aggregate particles (m) |

| | |
|---|---|
| $P_{\text{conv}}$ | Convex perimeter of the particle (m) |
| $S, L$ | Width and length of an aggregate particle (m) |
| $b_1$ | Fitting parameter of Eq. (14) |
| $b_2, b_3$ | Fitting parameter of Eq. (15) |
| $m_1, m_2$ | Fitting parameter of Eq. (16) |

## 1 Introduction

The presence of aggregates in cement-based composites (e.g. concrete) has gained insights from many scientific and engineering communities for many decades, and it is generally accepted that the size, shape, and texture of aggregates well influence the properties of the fresh and hardened mixtures. Recent studies have been conducted widely towards the influence of aggregate morphology, e.g. shape and size, on structural performances (Denis et al. 2002; Rocco and Elices 2009), transport properties (Krejsová et al. 2018; Santos et al. 2020; Ueno and Ogawa 2020), viscosity (Erdoğan et al. 2008; Westerholm et al. 2008), and flowability (Cui et al. 2020) of cement-based composites. The influences of aggregate size, content, and shape on effective properties are demonstrated. Several shape indices have been adopted, such as elongation, surface roughness, and fractal dimension, exhibiting notable effects on the mechanical responses (Wei et al. 2020). However, grain shapes of virtually packed granular porous media in existing numerical studies are mostly convex rather than concave, which is contrary to real particulate structures. In this study, we will discuss how realistic fractal shapes of aggregates affect effective transport properties, in particular ionic diffusion.

Effective diffusivity is one of the most important transport behaviours in terms of concrete durability issues (Gjørv 2011). The chloride-induced ionic transport in the cement-based composite is mainly driven by diffusion (Bastidas-Arteaga et al. 2011). Either bulk diffusion or migration tests have been developed to quantify the diffusion coefficient in the Fick's law (Luping and Gulikers 2007). In experiments, the diffusivities have been widely tested by considering the cement content (Pae et al. 2021), aggregate size distribution (Shafikhani and Chidiac 2019), and solid fractions (Delagrave et al. 1996). Especially for aggregate particles, their existence is to necessarily account for the tortuosity of diffusive paths (Patel et al. 2016). Image analysis (IA) is developed to determine the shape of coarse aggregates for the interpretation of aggregate geometrical parameters (e.g. elongation) (Fernlund 2005). It is intuitive that geometrical parameters can significantly affect the durability of the concrete (Kwan et al. 1999). However, few experiments targeting to correlate diffusivities and geometrical parameters have been conducted due to the limited control of particle morphology.

Effective diffusivity is analytically developed by upscaling from heterogenous to a continuous homogenous medium (Hornung 1996). The modification of Hashin–Shtrickman upper and lower bounds is derived for the effective diffusivity of the two-phase isotropic composite media; under the given aggregate fraction, these bounds are reached when the shape of inclusion in the matrix is sphere (Torquato and Haslach Jr 2002). Alternative solutions of effective diffusivity are based on effective medium approximation (EMA) (e.g. Maxwell and self-consistent approximations), which also account for simplified microscale information (Choy 2015; Hoch 2015). For instance, the homogenisation is applied to account for pore structures for the diffusivity of cement paste, and a self-consistent scheme

is adopted to evaluate the effective diffusivities in the cement-based composite. Also, multiscale modelling by *N*-layered spherical inclusion theory still assumes aggregates to be spheres (Sun et al. 2011). Therefore, it is desirable to develop the analytical model to account for geometrical parameters, besides the first-order approximation accounting for volume content and size of aggregates.

In addition to the theoretical approaches, several numerical methods are proposed to model the diffusivity in cement-based composites, such as Lattice Boltzmann method (LBM) (Zhang et al. 2012, 2014) and finite element method (FEM) (Idiart et al. 2011; Liu et al. 2012; Zheng et al. 2012; Xu and Li 2017; Xiong et al. 2020). LBM modelling is chosen to be an appropriate micro-solver for complex boundary problems, when the heterogeneity of cement paste (e.g. pore structures) is considered (Zhang 2013). However, parameters at pore scale were neglected in this study, and cement paste is assumed to be homogenous. FEM modelling is straightforwardly conducted for the diffusion study based on Fick's Law, where Monte Carlo algorithm has been widely applied to generate the meso-structure by construction of random packing with regular particle shapes (Du et al. 2014; Liu et al. 2014). Randomness (e.g. aggregate positions) is seldom quantitatively evaluated in the investigation on the effective diffusivity, though disordered inclusion positions in the matrix phase has been demonstrated to be one of influencing factors to the transport properties (Laubie et al. 2017a; Cui et al. 2019; Wang et al. 2019b). In numerical modelling, representative elementary volume (REV) size of the periodical structure for the aggregate packing is also a concern to the simulation (Zhou et al. 2014; Ma et al. 2016). Regardless of REV size, it has been found that diffusion profiles for different idealised convex aggregate shapes (e.g. square, regular pentagon, hexagon, and circle) are almost identical (Xiao et al. 2012). Representative aggregate shapes in most FEM modelling of diffusivity are usually oversimplified, which may not be able to represent the morphologies of real aggregates. It is found that aggregate elongation (e.g. for elliptical aggregates) can reduce effective diffusivity (Zheng et al. 2012, 2016). Nevertheless, due to the elongation, it is unclear to see how the orientation of elliptical aggregates affects the diffusivity variance (Abyaneh et al. 2013). In addition to elongation, 2D particle shape can be quantified by other traditional and scale-dependent geometrical parameters, such as roundness and roughness (Zheng and Hryciw 2015). Among these geometrical parameters, none of them is able to fully describing all aspects of morphology of the aggregate shape (Kwan et al. 1999). Fractal dimension has been introduced to be a novel global index summarising all geometrical characterises, and improved spherical harmonics based on the fractal dimension is used to construct the 3D irregular shape (Wei et al. 2018). Moreover, fast Fourier transformation (Mollon and Zhao 2012) and pixel-based method (Liu et al. 2018) are also alternative solutions to generate irregular shapes, which can be feed into numerical models with well-controlled shape indices to identify the key parameters and establish isolated cause–effect relations.

This study presents an FEM investigation on diffusivities of cement-based composites, emphasising on the effects of aggregate stochastics, in terms of spatial distributions, elongation, and morphology features. The main contents are outlined as follows. In Sect. 2, packing processes for the virtual concrete sample consisting of various of aggregate shapes are firstly introduced. The disorder index is introduced to quantitively measure the aggregate position randomness. Then, how the irregular aggregate is generated using Fast Fourier Transformation (FFT) via two compressed shape factors, relative roughness ($R_r$) and fractal dimension ($F_d$), is described. Subsequently, key details about FEM simulation of one-way steady-state diffusion based on Fick's first law are illustrated. Results and relevant discussions focusing on influencing factors on effective diffusivity, such as disorder index,

elongation, and aggregate shapes, are demonstrated in Sect. 3. Sensitivity study is also conducted for the relations between different length-scaled geometrical parameters of irregular aggregate and effective diffusivity. Inspired by the sensitivity study, a promising prediction model is proposed with only two shape parameters ($R_r$ and $F_d$) for specific aggregate fraction. Finally, some conclusions are drawn in Sect. 4.

## 2 Methods

For modelling the effective diffusivity of cement-based composites, mesoscale numerical samples consisted of the cement and aggregates should be established. It is noted that the grain size distribution of aggregates (or aggregate sieving) is also an important factor in transport properties and can be seen elsewhere (Caré 2003; Sun et al. 2011; Liu et al. 2018; Pollmann et al. 2021). Thus, the aggregate grading is not the focus of this study and only mono-sized aggregates are applied for isolating grading effects. The basic underlying assumption of this mesoscale level analysis is that only large aggregates in the same grading are explicitly represented in cementitious material, while the rest fine aggregates are represented as homogenous 'cement' paste. The fundamental parameters contributed to the construction of aggregates in cement paste in this study are the aggregate fraction, shapes, and spatial arrangement. For better understanding real aggregate porous structures, the coupled effect of aggregate size and morphology features will be studied in the future research.

### 2.1 Packing Structure of Aggregates

#### 2.1.1 Ordered Packing

To investigate the effect of aggregate shape on the effective diffusion, hexagonal packing is employed to construct 2D composite structures, in which aggregates with the same size are inserted into cement paste. The maximum solid fraction equal to $\frac{\sqrt{3}\pi}{6}$ can be achieved for 2D mono-sized circular packing (Hales 1992). The overall shape of the aggregates (e.g. elongation) is the dominant morphological parameter controlling packing structure (Hafid et al. 2016). The hexagonal packing can increase the aggregate spacing and avoid the aggregate overlaps for the other shapes (e.g. ellipse, polygon, and irregular shape).

Contact check is required to avoid the intersection between aggregates caused by the rotation of non-circular aggregates. For either polygonal or irregular aggregate, each vertex of shapes should be checked to determine whether it is contacted with others. It can be implemented by using the built-in function of *inpolygon* in MATLAB (Zhang et al. 2017). Meanwhile, to guarantee at least one-mesh size space between aggregates, the aggregate area for contact check is 2% more than the targeted aggregate area. The choice of REV and hexagonal packing results in 120 aggregates in the sample. Each taken aggregate at the position of hexagonal packing is randomly rotated and placed into REV size of cement paste. Geometrical periodicity is ensured in both horizontal and vertical directions.

#### 2.1.2 Disordered Packing

In terms of the disordered packing, only circular shape is used to check the effects from the spatial arrangement of aggregates. The way to quantitively describe the overall effect

of aggregate position is based on the original disorder index $I_d$ (Laubie et al. 2017a). It not only affects the mechanical properties (Laubie et al. 2017a, b), but also impacts the fundamental understanding of fluid transport properties (Holtzman 2016; Fantinel et al. 2017). However, the original disorder index $I_d$ tends to ignore the small perturbations, which is less sensitive to the specific solid mechanics problems. As the Voronoi tessellation is quite sensitive to such small disturbances, the disorder index $I_v$ modified to cooperate with Voronoi tessellation is used in this paper. It can be defined as (Cui et al. 2019):

$$I_v = \sqrt{\frac{\sum_{k=1}^{N_a} \left(\phi_k - \phi\right)^2}{N_a - 1}}, \tag{1}$$

where $N$ is the number of aggregates in the domain of cement paste, $\phi_k$ is local solid fraction within the Voronoi cell, $\phi$ is the overall solid fraction in the cement paste.

Disordered packing is introduced by Monte Carlo movement of each circular based on the initial hexagonal packing (Wang et al. 2019b). To stabilise the $I_v$ around a specific value, sufficient iterations are required to assure the uncertainty less than 5%.

### 2.2 Generation of Aggregate Shapes With Multi-Scale Morphology Features

Mesoscale models of cement-based composites are usually generated with regular shapes, such as circle, ellipse and polygon (Du et al. 2014). To construct more realistic aggregate morphology, discrete Fourier transform of the contour of the grain can be used (Mollon and Zhao 2012). In the 2D case, with the aggregate particle centre $O$, the contour of the aggregate particle is discretised by $N_p$ points $P_i$, with a constant polar angle $\theta_P = 2\pi/N_P$. The distance between $P_i$ and $O$ is defined as $l_i$, and the discrete signal $l_i(\theta_i)$ can be expressed by:

$$l_i\left(\theta_i\right) = l_0 + \sum_{n=1}^{N} \left[X_n \cos\left(n\theta\right) + Y_n \sin\left(n\theta\right)\right] \tag{2}$$

where $n$ is the number of discrete signal, $N$ is the total number of discrete signal and equal to 64 in the present study (Wang et al. 2019a), and $l_0$ is the average of discrete signals. The spectrum $X_n$ and $Y_n$ of the discrete signal after Fourier transformation is defined as:

$$X_n = \frac{1}{N} \sum_{i=1}^{N} \left[l_i \cos\left(i\theta_i\right)\right] \tag{3}$$

$$Y_n = \frac{1}{N} \sum_{i=1}^{N} \left[l_i \sin\left(i\theta_i\right)\right] \tag{4}$$

The most sensitive term to the irregular shape is normalised amplitude $F_n$ for each discrete signal number $n$, defined as:

$$F_n = \frac{\sqrt{X_n^2 + Y_n^2}}{p_0}, \tag{5}$$

For $n = 0$, $F_0$ is normally set to 1 for the normalisation. $F_n$ for $n = 1$ is equal to 0 ensuring that the aggregate is centred at the position of point $O$. $F_2$ controls the elongation of

aggregate particles, and $F_n$ for $3 \leq n < 8$ are used to represent irregularity of aggregates while $F_n$ for $n \geq 8$ are related to the roughness of the particle surface. For natural aggregates, normalised amplitude $F_n$ is roughly linearly decreased with the discrete signal number $n$. This linear relationship can be denoted with the combination of fractal dimension $F_d$ for $n \geq 2$ in the log–log scale, which is a global geometrical index describing the aggregate shape at multiscale (Wei et al. 2018). The exponential relation between the normalised amplitude $F_n$ and discrete signal number $n$ can be expressed by:

$$F_n \propto n^{-2H}, \tag{6}$$

where $-2H$ is the slope of $\log(F_n)$ and $\log(n)$, and $H$ is the Hurst coefficient associated with fractal dimension $F_d$,

$$F_d = 2 - H. \tag{7}$$

Therefore, the normalised amplitude $F_n$ can be modified with $F_d$ for $n \geq 2$, defined as:

$$F_n = F_2\left(\frac{n}{2}\right)^{2F_d-4}. \tag{8}$$

The relative roughness $R_r$ can be used to compute how globally different the irregular aggregate shape is from $l_0$ determined equivalent circle (Wei et al. 2020). $R_r$ derived from Fourier series is deduced in Appendix 1 and defined as:

$$R_r = \sqrt{\sum_{n=2}^{\infty}\left(F_2^2\left(\frac{n}{2}\right)^{4F_d-8}\right)}. \tag{9}$$

The influence of $F_d$ and $R_r$ on the morphology of irregular shape is illustrated in Fig. 1a. It has been found that both increases in $F_d$ and $R_r$ result in more fractal shape with rougher surfaces.

### 2.3 FEM Modelling Effective Diffusivity

The finite element method (FEM) is applied to simulate the one-way steady-state diffusion based on Fick's first law, shown as:

$$J = -D_{\text{eff}}\frac{\mathrm{d}c}{\mathrm{d}x}, \tag{10}$$

where $J$ is the total diffusion flux ($\text{mol}/\text{m}^2/\text{s}$), $\frac{dc}{dx}$ is the concentration gradient ($\text{mol}/\text{m}^4$), and $D_{\text{eff}}$ is the effective diffusivity($\text{m}^2/\text{s}$). As reported by Savvas et al. (2016), simulation results of cement-based composite properties can be influenced by the selection of REV size. With the increasing volume of the cement-based structure, the dispersion or fluctuation of studied properties becomes small or less influenced by the size of REV (Zhou et al. 2014; Savvas et al. 2016; Xu et al. 2017). In terms of effective diffusivity, regardless of aggregate shapes, RVE size is determined to be at least 5 times larger than the maximum size of aggregates (Liu et al. 2018). For this study, numerical simulation of steady-state diffusion is conducted. As previous studies report that cement diffusivity is around the order of $10^{-12}\text{m}^2/\text{s}$ (Page et al. 1981, 1995; Yu and Page 1991; Luping and Nilsson 1993; MacDonald and Northwood 1995; Pivonka et al. 2004), the diffusion coefficient of cement is

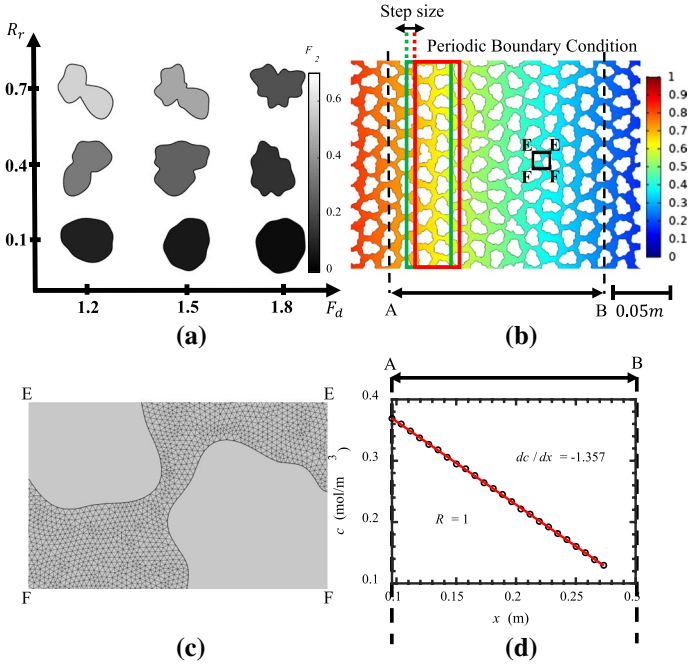


**Fig. 1** **a** Variation in irregular shapes with fractal dimension $F_d$ and relative roughness $R_r$, **b** illustrations of FE diffusivity modelling of 2D hexagonal packing of irregular aggregate with $F_d = 1.65$ and $R_r = 0.357$, **c** mesh layout, and **d** concentration profile along the horizontal displacement

set here as $D_c = 1 \times 10^{-12} \mathrm{m}^2/\mathrm{s}$, within the same range of other relevant numerical studies (Pan et al. 2015; Ruan et al. 2019). The diffusion coefficient of aggregate $D_a = 0 \mathrm{m}^2/\mathrm{s}$ is assumed due to its impermeable nature. The REV size is considered as 10 times of the maximum aggregate size, as shown in Fig. 1b, to compute more stable value of effective diffusivity $D_{\mathrm{eff}}$ and save the computational efforts.

In Fig. 1b, irregular aggregates with $F_d = 1.65$ and $R_r = 0.357$ are packed in REV size of cement at the solid fraction of 50%, and it has been chosen as an example to illustrate the numerical simulation of effective diffusivity. More details of aggregate packing in REV size of cement paste will be introduced in the following section. To eliminate the influence of value fluctuation at the boundary, REV size of geometry is doubled in the diffusion direction. The chloride concentration at left boundary is set as 1 $\mathrm{mol}/\mathrm{m}^3$, while it is set as 0 $\mathrm{mol}/\mathrm{m}^3$ at the right end. Meanwhile, periodical boundary conditions have been given on the top and bottom boundary. The mesh layout, particularly for the space between irregular shape, is shown in Fig. 1c, where the relative mesh size (the ratio of mesh size to aggregate size in diameter) is less than 0.03. $D_{\mathrm{eff}}$ is computed from the middle section to minimise the boundary effects.

This middle section (A–B) of the samples can be homogenised by setting up a moving window with the width of about 3 area-equivalent circle diameters of aggregate. Note that all aggregates in cement paste are of the same area. The window is moved by a step size of 1/5 of its length for calculating concentration, $c$, at the horizontal displacement, $x$. The reference evolution of concentration gradient, $\frac{\mathrm{dc}}{\mathrm{dx}}$, is shown in Fig. 1d. Meanwhile, the total flux $J$ for this middle section can be computed from FE software COMSOL to calculate the

value of effective diffusivity, $D_{\text{eff}}$. In following sections, to eliminate the influence of cement diffusivity value on our results,$D_{\text{eff}}$ is normalised via $\frac{D_{\text{eff}}}{D_0}$, where $D_0$ is the effective diffusivity of the hexagonal packing of circular aggregates.

## 3 Results and Discussion

### 3.1 Spatial Distribution of Aggregates

Randomness of aggregate positions due to Monte Carlo iterative movement is characterised by$I_v$. It is controlled by apparent diameter $d_{\text{ap}} = \gamma d$ with associated $\gamma \in [1, \frac{\sqrt{3}\pi}{6}]$, where $d$ is the original diameter of circular aggregate. Note that when $d_{\text{ap}}$ reaches to the maximum at$\gamma = \frac{\sqrt{3}\pi}{6}$, circular aggregates are placed in the hexagonal packing. To compute the variation in $\frac{D_{\text{eff}}}{D_0}$ with $I_v$, 100 disordered spatial distributions of circular aggregates at $I_v \in [0.01, 0.06]$ are generated at $\phi = 50\%$. Figure 2a shows an example of the FEM modelling for a random packing of circular aggregates at $I_v = 0.0387$. The throat size between two grains is defined as the shortest distance between points on each neighbour grain boundaries. Figure 2b presents probability density function (PDF) of relative throat size, defined as the ratio of throat size to circular aggregate diameter, at $I_v = 0, 0.0163, 0.0387$ and 0.0565. The corresponding standard deviations of lognormal fittings for them are: $\sigma_{\text{rt}} = 0, 0.075, 0.221$, and 0.374. The higher $I_v$ induces the larger $\sigma_{\text{rt}}$ due to the wider range

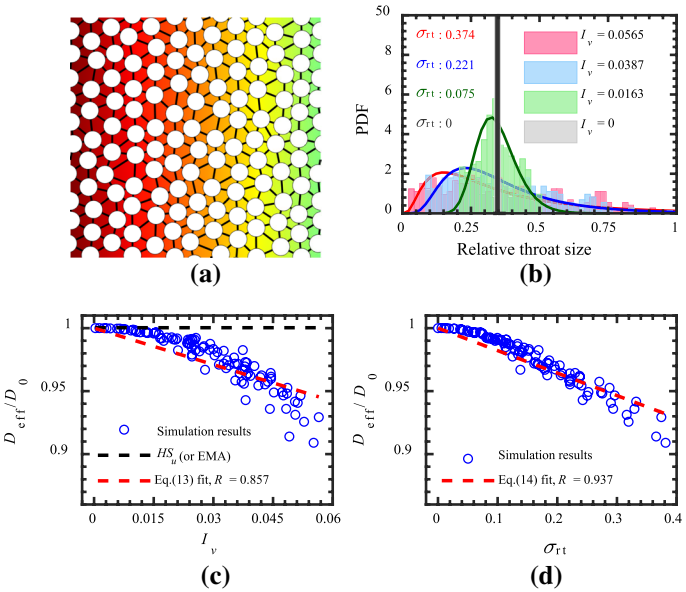


**Fig. 2** **a** FE modelling results for random packing of circular aggregates at $I_v = 0.0387$, and black solid lines denote throats between circular aggregates, **b** histogram of probability density function (PDF) of relative throat sizes at $I_v$ of 0, 0.0163, 0.0387, and 0.0565 and their corresponding plots of lognormal distribution fitting in black, red, blue, and green solid lines, and each fitting is given with the standard deviation of relative throat size $\sigma_{\text{rt}}$, **c** relations between $\frac{D_{\text{eff}}}{D_0}$ and $I_v$ at solid fraction $\phi$ of 50%, and $HS_u$(or EMA) is the Hashin–Shtrikman upper bound of Eq. (11) at $\phi$ of 50%, and **d** relations between $\frac{D_{\text{eff}}}{D_0}$ and standard deviation of relative throat size distribution $\sigma_{\text{rt}}$

of throat sizes. After involving in all disordered packings, Fig. 2c indicates the relation between $\frac{D_{\text{eff}}}{D_0}$ and$I_v$. For the diffusivity of two-phase composite of which aggregate phases are impermeable, the well-known narrow Hashin–Shrinkman (HS) upper bound, derived by the variational theorems (Hashin and Shtrikman 1962), is

$$HS_u(\phi) = \frac{D_c}{(1+\phi)D_0}. \tag{11}$$

More information about the derivation can be referred to Appendix 2. Notably, $HS_u$, defined the same as EMA in terms of Maxwell approximation for 2D effective diffusivity (Jóhannesson and Halle 1996; Torquato and Haslach Jr 2002), is shown in Fig. 2c. At $I_v = 0$, $HS_u$ well matches our simulation result, while $\frac{D_{\text{eff}}}{D_0}$ decreases obviously with the increase in $I_v$ and below the $HS_u$. As $I_v \in [0.01, 0.06]$, $\frac{D_{\text{eff}}}{D_0}$ fluctuates within a range of around 10%. Since $I_v$ is quite sensitive to throat size, the relation between $\frac{D_{\text{eff}}}{D_0}$ and $\sigma_{\text{rt}}$ is also shown in Fig. 2d, where $\frac{D_{\text{eff}}}{D_0}$ generally decreases with the increase in $\sigma_{\text{rt}}$. Evidently, $\frac{D_{\text{eff}}}{D_0}$ can be correlated with $I_v$ or $\sigma_{\text{rt}}$. For the simplicity, when $I_v \in [0.01, 0.06]$ and $\sigma_{\text{rt}} \in [0, 0.4]$, both correlations in Fig. 2c and d are defined by linear fittings, starting from $\frac{D_{\text{eff}}}{D_0} = 1$ at $I_v = 0$ and $\sigma_{\text{rt}} = 0$:

$$\frac{D_{\text{eff}}}{D_0}(I_v) = a_1 I_v + 1, \tag{12}$$

$$\frac{D_{\text{eff}}}{D_0}(\sigma_{\text{rt}}) = a_2 \sigma_{\text{rt}} + 1, \tag{13}$$

where $a_1 = -0.956$ and $a_2 = -0.177$ are fitting parameters. Other nonlinear fitting functions may provide better approximations for the data presented, while more fitting parameters will be involved. Relative to the $I_v$, $\sigma_{\text{rt}}$ is a more effective factor to determine effective diffusion because of its higher correlation coefficient.

### 3.2 Aggregate Elongation

To investigate the influence of elongations on the degree of effective diffusivity, elliptical aggregate is preferred to isolate other geometry factors. With the packing process described in Sect. 2 in hand, different $\phi$ (e.g. 30, 35, 40, 45, and 50%) is readily achieved. For each $\phi$, the number of aggregates and aggregate size are kept the same in the hexagonal packing. Meanwhile, elongations from 0.5 to 1 with an increment of 0.02 are selected, where the elongation of 1 means circular aggregate. Notably, all the elliptical aggregates, placed in the hexagonal packing, with the same elongation can be rotated randomly within $\theta \in [0, \pi]$ without contacting each other. Figure 3a shows an example of FEM modelling results for the hexagonal packing of elliptical aggregates with the elongation (*El*) of 0.7 at the $\phi$ of 50%. Figure 3b shows the probability density function of relative throat size at *El* of 0.5, 0.7, 0.9, and 1. Meanwhile, the standard deviation of relative throat size, $\sigma_{\text{rt}}$, approximated by lognormal distribution, increases with smaller *El*.

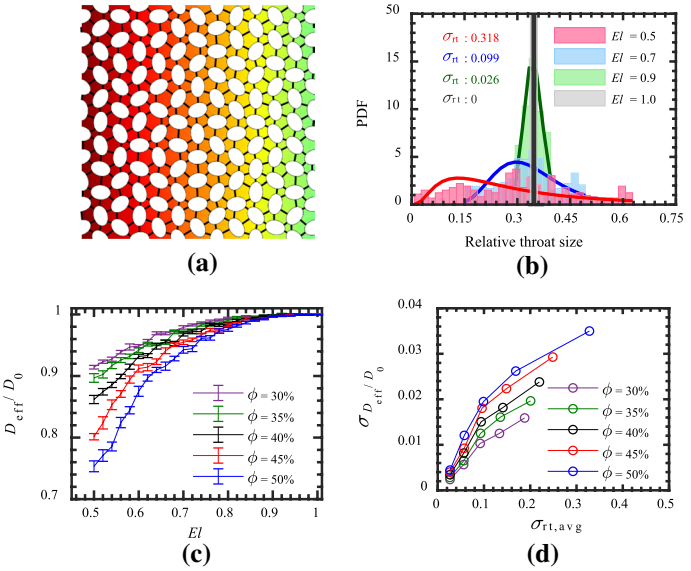


**Fig. 3** **a** FE modelling results for the hexagonal packing of elliptical aggregate with elongation (*El*) of 0.7 at solid fraction $\phi$ of 50%, where black solid lines mean throat sizes between elliptical aggregates, **b** histogram of probability density function (PDF) of relative throat sizes at *El* of 0.5, 0.7, 0.9, and 1, and corresponding plots of lognormal distribution fitting in red, blue, green, and black solid lines with the standard deviation of relative throat size distribution $\sigma_{rt}$, **c** relations between $\frac{D_{eff}}{D_0}$ and *El* at $\phi$ of 30, 35, 40, 45, and 50%, and **d** relation between standard deviation of effective diffusivities $\sigma_{\frac{D_{eff}}{D_0}}$ and average value of all standard deviation of relative throat size distribution $\sigma_{rt,\,avg}$ at $\phi$ of 30, 35, 40, 45, and 50%, and five points at the same $\phi$ are referred to values at the elongation of 0.9, 0.8, 0.7, 0.6, and 0.5 from left to right. Note that elongation *El* for the elliptical aggregate is defined as the ratio of width (the short axis) to length (the long axis), consistent with the definition in Table.1

All FEM modelling results, in terms of $\frac{D_{eff}}{D_0}$ versus *El*, are illustrated in Fig. 3c, where each error bar is calculated from 15 samples at each *El* increment. It is found that at each $\phi$, $\frac{D_{eff}}{D_0}$ is decreased with the smaller elongation, which is consistent with those in previous studies (Zheng et al. 2012, 2016; Abyaneh et al. 2013). This tendency becomes more obvious at larger $\phi$. At $\phi$ of 50%, *El* of 0.5 even causes around 25% reduction in $\frac{D_{eff}}{D_0}$ compared with circular inclusions. From error bars, it is also found that the smaller elongation causing a wider range of throat size induces the larger fluctuation in $\frac{D_{eff}}{D_0}$. To further investigate the elongation induced fluctuation in $\frac{D_{eff}}{D_0}$, at each *El* 50 samples are used, of which the standard deviation of effective diffusivities, $\sigma_{\frac{D_{eff}}{D_0}}$, and the average value of all standard deviations of relative throat size distribution, $\sigma_{rt,\,avg}$, are computed. In Fig. 3d, $\sigma_{\frac{D_{eff}}{D_0}}$ is plotted with $\sigma_{rt,\,avg}$ at different $\phi$, which indicates smaller $\sigma_{rt,avg}$ causes the smaller $\sigma_{\frac{D_{eff}}{D_0}}$. When considering random orientation angles, elliptical aggregates with the larger *El* tend to be closer to circular aggregates, resulting in $\sigma_{rt,avg}$ closer to zero and more stable $\frac{D_{eff}}{D_0}$. In addition, it is more obvious both *El* and $\phi$ influence $\sigma_{\frac{D_{eff}}{D_0}}$ much. In the conditions of smaller *El*, aggregate fractions can much vary $\frac{D_{eff}}{D_0}$ and induce higher $\sigma_{\frac{D_{eff}}{D_0}}$. When aggregate fraction is very lim-

ited (e.g. $\phi \approx 0$), $\sigma_{\frac{D_{\text{eff}}}{D_0}}$ is nearly zero regardless of the rotation angles. Furthermore, at *El* of 0.5 and $\phi$ of 50%, $\sigma_{\frac{D_{\text{eff}}}{D_0}}$ shows the maximum value less than 4%, which is a very small disturbance compared to the elongation induced reduction in $\frac{D_{\text{eff}}}{D_0}$ (around 25%). Based on the above discussions, especially for composites of high solid fractions, small aggregate elongation can cause an obvious reduction in effective diffusivity, in which the fluctuation can be ignored.

### 3.3 Global Aggregate Morphology Features

Circular, polygonal, elliptical, and irregular aggregates are used to investigate the influence of aggregate shapes on $\frac{D_{\text{eff}}}{D_0}$ at $\phi \in [30\%, 50\%]$ with an increment of 5%. For each $\phi$ of packings contained distinctively shaped inclusions, aggregate area is the same. To perform this investigation more accurately, it is necessary to eliminate influences of aggregate spatial distributions and elongations. Mass centres of aggregates in different cases are at the same position of standard hexagonal packing. Meanwhile, irregular and elliptical aggregates have the same *El*s (e.g. around 0.7) and orientation angles.

In Fig. 4, it can be found that an increase in $\phi$ causes a decrease in $\frac{D_{\text{eff}}}{D_0}$ for all shapes of aggregates, which is quite consistent with Li et al. (2012). Meanwhile, 2D $HS_u$ is perfectly matched with $\frac{D_{\text{eff}}}{D_0}$ for the hexagonal packing of circles at $\phi$ of 30–50%, proving the efficiency of our simulation results. It is also found that $\frac{D_{\text{eff}}}{D_0}$ values for circular, polygonal, and elliptical aggregates are close to each other but still with slight differences, similar to relevant studies (Du et al. 2014; Jie et al. 2017). However, the polygonal aggregate causes a slightly lower $\frac{D_{\text{eff}}}{D_0}$ than circular aggregates, due to smaller sized throats caused by sharp corners around its circumference. There is also a very small fluctuation ($< 1\%$) of $\frac{D_{\text{eff}}}{D_0}$ for polygonal aggregates, since the cement-based structure with polygonal aggregates is slightly different from each other due to random rotation angles and length of polygonal aggregates. Elliptical aggregates display a little smaller $\frac{D_{\text{eff}}}{D_0}$ than polygonal and circular aggregates, that is, because the elliptical aggregate is a more elongated aggregate and randomly orientated. Furthermore, as $\phi$ increases, it is more apparently seen that the irregular

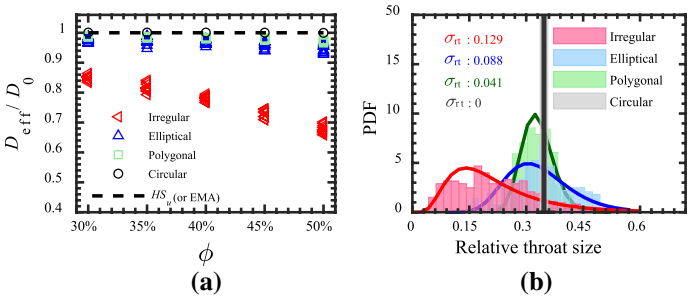


**Fig. 4** **a** Influence of aggregates shapes on effective diffusivities $\frac{D_{\text{eff}}}{D_0}$ at the solid fraction $\phi$ of 30, 35, 40, 45, and 50%, where $F_d = 1.85$ and $R_r = 0.99$ are used to generate the irregular aggregates, and *El* of each irregular shape is slightly varied around 0.7; **b** probability density function (PDF) of relative throat sizes of irregular, elliptical, polygonal, and circular aggregates at $\phi = 50\%$, and corresponding plots of lognormal distribution fitting in red, blue, green, and black solid lines

**Table 1** List of geometric parameters for regression studies

| Feature No | Feature name | Feature definition |
|---|---|---|
| 1 | Fractal dimension ($F_d$) | Equation (7) |
| 2 | Relative roughness ($R_r$) | Equation (9) |
| 3 | Elongation | $\frac{S}{L}$ |
| 4 | Circularity | $\sqrt{\frac{r_{\text{insc}}}{r_{\text{circ}}}}$ |
| 5 | Area sphericity | $\frac{A_s}{A_{\text{cir}}}$ |
| 6 | Perimeter sphericity | $\frac{P_c}{P_S}$ |
| 7 | Diameter sphericity | $\frac{d_c}{d_{\text{cir}}}$ |
| 8 | Roundness | $\frac{\sum r_c}{n_c r_{\text{insc}}}$ |
| 9 | Regularity | $\text{Log}\left(\frac{P_s}{P_s - P_{\text{conv}}}\right)$ |

aggregate shows much smaller $\frac{D_{\text{eff}}}{D_0}$ than other regular shapes (e.g. circle, polygon, and ellipse). At the $\phi$ of 50%, when irregular and elliptical aggregates are placed at the same position with the same elongation and orientation angles, irregular aggregate still results in around 30% reduction in $\frac{D_{\text{eff}}}{D_0}$. The main reason is that only irregular aggregates in this study contain the concave shapes, increasing the effective length of diffusive path, due to decreasing the average and enlarging the scope of relative throat size (Fig. 4b). Furthermore, similar to previous discussion in Sect. 3.2, elongation-induced fluctuation in $\frac{D_{\text{eff}}}{D_0}$ can also be negligible when compared to concave shape-induced reduction in $\frac{D_{\text{eff}}}{D_0}$.

Previous experimental studies (Caré 2003; Sun et al. 2011; Pollmann et al. 2021) have investigated influences of aggregate size on effective diffusivity. They show that the reduction in $\frac{D_{\text{eff}}}{D_0}$ can be up to 40% at $\phi = 50\%$ with wider aggregate size distribution. Although only mono-sized aggregate is covered in our simulation, as illustrated in Fig. 4a it is surprising that $\frac{D_{\text{eff}}}{D_0}$ can decrease by about 30%, at $\phi = 50\%$ of realistic aggregate convex shapes. Such a comparable reduction in $\frac{D_{\text{eff}}}{D_0}$ inspires us to explore quantitative relations between it and shape indices in Sect. 3.4.

### 3.4 Correlating Shape Indices to Effective Diffusivity

With the development of high-resolution cameras, 2D aggregate outline is of very easy access to be achieved. It is very promising to correlate 2D shape indices to effective diffusivity in cement composites. As previous illustration, the morphology of the irregular aggregate is generated just by two compressed factors, $F_d$ and $R_r$. $F_d$ is a global geometrical parameter introducing how the morphology feature is altered at every length scale. $R_r$ is another geometrical index to describe the overall irregularity of aggregates, which defines how the irregular shape is different from the area-equivalent circle. Other common single-length geometrical parameters are also included to describe the morphology of irregular shape, as shown in Table. 1. In Guida et al. (2020), three non-dimensional shape parameters are introduced over the range of experimentally accessible scales: (i) aggregate shape at the macro-scale, (ii) aggregate roundness at the mesoscale, and (iii) aggregate texture (surface roughness) at the micro-scale. The overall form carries information on the

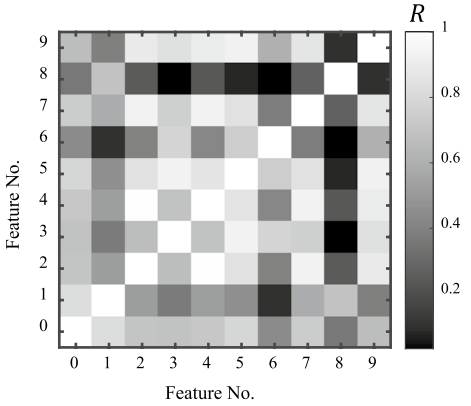


**Fig. 5** A heatmap of correlation between a different pair of features. Feature 0 is $\frac{D_{\text{eff}}}{D_0}$, and other feature numbers refer to Table 1. Notations: $A_s$ is the projected area of an aggregate particle ($\text{m}^2$); $A_{\text{cir}}$ is the area of the minimum circumscribing circle ($\text{m}^2$); $d_c$ is the diameter of a circle having the same projected area as the particle ($m$); $d_{\text{cir}}$ is the diameter of the minimum circumscribing circle ($m$); $r_{\text{circ}}$ is the radius of the minimum circumscribing circle ($m$); $P_c$ is the perimeter of a circle having the same projected area as the particle ($m$); $r_{\text{insc}}$ is the radius of the largest inscribed circle in the particle ($m$); $r_c$ is the radius of the circles that approximate the corners of the particles contour ($m$); $P_S$ is the perimeter of the aggregate particles ($m$); $P_{\text{conv}}$ is the convex perimeter of the particle ($m$); $S$ and $L$ are the width and length of an aggregate particle ($m$). Note that among all trial rectangular bounding boxes with orientations ranging over $180^{\circ}$ to circumscribe the irregular shape, the one with the longest dimension is used to define both the width and length of the irregular shape (Zheng and Hryciw 2015)

proportions of the particle, i.e. how isometric or elongated the particle is; roundness (angularity) accounts for local features of the aggregates (Wadell 1932; Ferellec et al. 2008). Furthermore, similar to Guida et al. (2020), three scale-dependent shape factors, such as sphericity, roundness, and roughness, have been defined, and the sphericity has been defined in five ways including area sphericity, diameter sphericity, circle ratio sphericity, perimeter sphericity, width-to-length ratio sphericity (or elongation) (Zheng and Hryciw 2015). According to Mollon and Zhao (2012), regularity can be used to measure the roughness alternatively. Sensitivity studies are performed to inspect the correlation with $\frac{D_{\text{eff}}}{D_0}$ in the following.

For the sensitivity study, $F_d$ is controlled to be varied from 1.05 to 1.85 with the increment of about 0.04, and $R_r$ is varied from 0.06 to 0.99 with an increment of about 0.05. Meanwhile, for the existence of irregular aggregates in hexagonal packing at $\phi$ of 50%, only 179 pairs of $F_d$ and $R_r$ with $F_2$ no more than 0.26 are selected, as $F_2$ mainly controls the elongation of irregular aggregates. After that, the linear regression analysis is needed to calculate the correlation indices between geometrical parameters and $\frac{D_{\text{eff}}}{D_0}$.All possible geometrical parameters discussed above are summarised in Table 1, all of which are less or more correlated with each other (Mora and Kwan 2000). Furthermore, sensitivity studies between geometrical parameters are conducted. The heatmap in Fig. 5 lists the score of correlation for each pair of features.

From Fig. 5, Features 3–9 are referred to the mostly used classical single-length-scale geometrical parameters, where Features 3–7 describe the forms of irregular aggregate in five different ways as in previous discussion (Zheng and Hryciw 2015). Among these five different forms (Features 3–7), they are almost highly correlated with each other, except for the correlation between perimeter sphericity (Feature 6) and diameter sphericity (Feature 7).

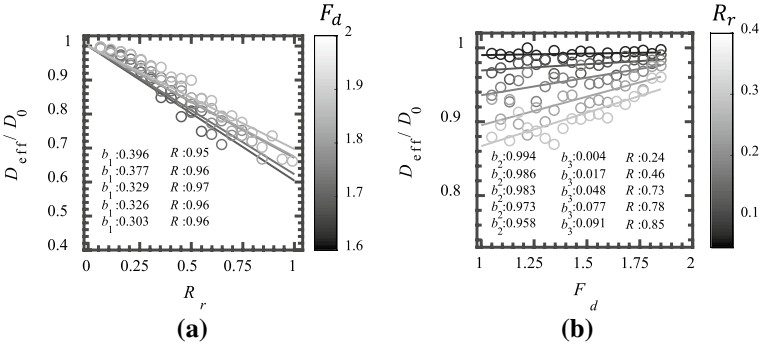


**Fig. 6** **a** Relation between $R_r$ and $\frac{D_{eff}}{D_0}$ at $F_d \in [1.65, 1.85]$ with the fitting of Eq. (14) and **b** relation between $F_d$ and $\frac{D_{eff}}{D_0}$ at $R_r \in [0.06,0.26]$ with fitting of Eq. (15)

Furthermore, roundness (Feature 8) is almost rarely correlated with these five different descriptions about forms (Features 3–7). That is also consistent with the previous statement that roundness is one of the three scale-dependent geometrical factors (Zheng and Hryciw 2015). Also, regularity (Feature 9) to characterise the surface roughness of irregular aggregate should be independent of these five aspects of forms (Features 3–7) and roundness (Feature 8). However, it is found to be correlated with five different forms (Feature 3–7). Look back to the definition of regularity, in which perimeter is included; thus, it is for general shape in the length scale of form, which is larger than roundness. While roughness denotes geometry smaller than roundness, we claim that regularity is not appropriate to describe roughness, contradicting Guida et al. (2020). Geometrical parameters except for perimeter sphericity (Feature 6) and roundness (Feature 8) are relatively highly sensitive to the $\frac{D_{eff}}{D_0}$ (Feature 0). $F_d$ and $R_r$ are the two most sensitive shape indices to effective diffusivity.

As in Eq. (9), $F_d$ and $R_r$ are independent of each other and able to describe the morphology of the irregular aggregate shape at multiscale by including all traditional geometrical parameters. Furthermore, either $F_d$ (Feature 1) or $R_r$ (Feature 2) also highly correlated with $\frac{D_{eff}}{D_0}$ (Feature 0). This indicates that the prediction equation of $\frac{D_{eff}}{D_0}$ can be effectively deduced only using $F_d$ and $R_r$ without including other shape factors. Therefore, $\frac{D_{eff}}{D_0}$ (Feature 0) due to the irregular aggregate will be further analysed only with $F_d$ (Feature 1) and $R_r$ (Feature 2) in the following part.

Here we take $\phi = 50\%$ as an example, of which the derivation process can be extended to $\phi$ of other values. In Fig. 6a and b, $R_r$ versus $\frac{D_{eff}}{D_0}$ at $F_d \in [1.65,1.85]$ and $F_d$ versus $\frac{D_{eff}}{D_0}$ at $R_r \in [0.06,0.26]$ are selected to plot. As $R_r \to 0$, irregular aggregates become circular, causing $\frac{D_{eff}}{D_0} \to 1$. Furthermore, the maximum value of $F_d$ is restricted to 2 in Eq. (7), because of our 2D studies. We apply the linear fitting of each relation:

$$\frac{D_{\text{eff}}}{D_0}\left(R_r\right) = 1 - b_1 R_r \tag{14}$$

$$\frac{D_{\text{eff}}}{D_0}\left(F_d\right) = b_2 - b_3\left(2 - F_d\right), \tag{15}$$

where$b_1$, $b_2$, and $b_3$ are fitting parameters. For negative correlation between $R_r$ and $\frac{D_{\text{eff}}}{D_0}$ shown in Fig. 6a, the correlation coefficients of each fitting are all above 0.9. Note that the $b_1$ value is increased at the larger$F_d$. For $F_d$ versus$\frac{D_{\text{eff}}}{D_0}$, linear fitting shows a small correlation coefficient of $R$ at small$R_r$. At$R_r \to 0$, indicating irregular grain shapes approximate circular, the decreases in the $F_d$ show the small fluctuation below$\frac{D_{\text{eff}}}{D_0} = 1$. As $R_r$ increases, Fig. 6b shows a more apparent positive correlation between $F_d$ and $\frac{D_{\text{eff}}}{D_0}$. Furthermore, $b_3$ is increased at larger$R_r$. In addition, $b_3$ value is decreased as increased $R_r$ causes aggregate shape more irregular. Both $b_2$ and $b_3$ in Eq. (15) are dependent on$R_r$, while only $b_1$ in Eq. (14) is dependent on$F_d$. Therefore, by combining the two, the relation between$F_d$, $R_r$, and $\frac{D_{\text{eff}}}{D_0}$ can be simply defined as:

$$\frac{D_{\text{eff}}}{D_0}\left(F_d, R_r\right) = 1 - \left(m_1 + m_2\left(2 - F_d\right)\right)R_r \tag{16}$$

where $m_1 = 0.286$ and $m_2 = 0.230$ are two fitting parameters. Among all 179 generated two-phase composites, the relation between $F_d$ and $R_r$ and $\frac{D_{\text{eff}}}{D_0}$ in Fig. 7a shows that increasing both $F_d$ and $R_r$ can even result in an almost 40% reduction in $\frac{D_{\text{eff}}}{D_0}$ at $\phi = 50\%$. Also, the plane fitting of Eq. (16) has the correlation coefficient $R = 0.948$, which proves fitting

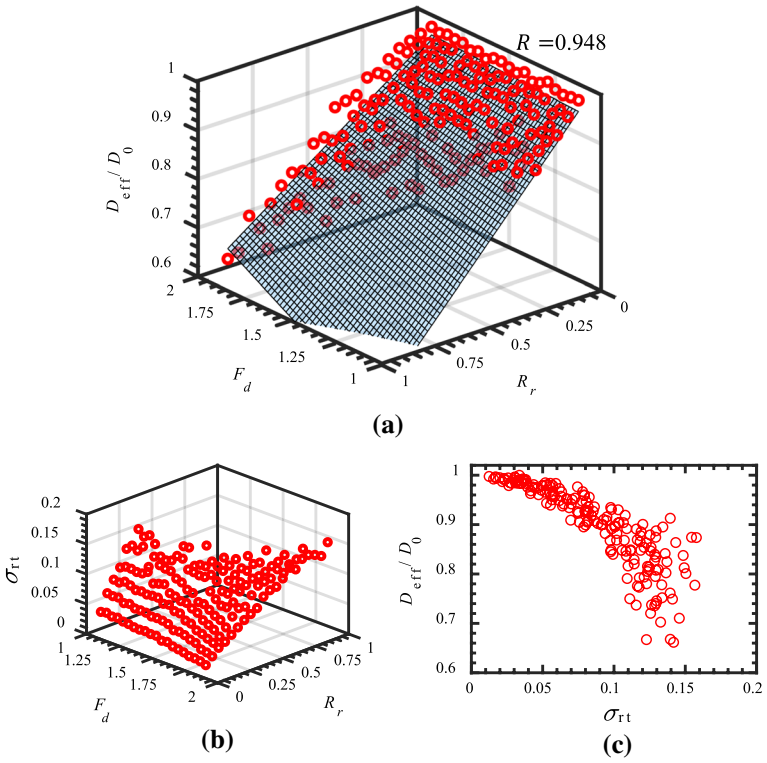


**Fig. 7** **a** 3D plot of relation between, $R_r$ and $\frac{D_{\text{eff}}}{D_0}$ with the plane fitting of Eq. (16), and **b** 3D plot of relation between $F_d$, $R_r$, and $\sigma_{\text{rt}}$ and **c** plot of $\sigma_{\text{rt}}$ and $\frac{D_{\text{eff}}}{D_0}$

accuracy as well as the strong correlation of $F_d$ and $R_r$ to $\frac{D_{\text{eff}}}{D_0}$. It can be further explained that due to the throat size influenced by the concave shape, the standard deviation of relative throat size distribution $\sigma_{\text{rt}}$ for irregular aggregate is also dependent on $F_d$ and $R_r$, as in Fig. 7b. It can be found that $\sigma_{\text{rt}}$ is decreased by an increase in $F_d$ and decrease in $R_r$. Furthermore, the relation $\sigma_{\text{rt}}$ and $\frac{D_{\text{eff}}}{D_0}$ in Fig. 7c shows that an increase in $\sigma_{\text{rt}}$ causes the decrease in $\frac{D_{\text{eff}}}{D_0}$. Therefore, $\frac{D_{\text{eff}}}{D_0}$ is highly affected by both $F_d$ and $R_r$, which change the morphology of aggregate shape and further change the throat size for diffusive paths, as in Fig. 4b.

## 4 Conclusion

In this study, the steady-state diffusion is modelled through FEM using Fick's first law. The influence of aggregate characteristics on the effective diffusivity of the cement-based composite has been specifically investigated. Compared with other relevant studies, where only convex aggregate shapes are considered, we take more realistic concave shapes depicted by FFT into consideration. Main conclusions of this study can be drawn as:

- More disordered packing has a larger standard deviation of throat size distribution. Larger disorder index and standard deviation of throat size distribution both induce the lower effective diffusivity, while throat size is more sensitive to and the first factor determining effective diffusivity.
- Lower aspect ratio contributes to decreasing effective diffusivity, especially at the higher aggregate fraction. Furthermore, smaller aspect ratio causes the larger standard deviation of relative throat size distribution, resulting in larger fluctuation in effective diffusivity. However, when compared with the reduction in effective diffusivity induced by low elongation, the fluctuation can be negligible.
- The irregular aggregate with the concave shape causes significantly smaller (e.g. even to about 30%) effective diffusivity than the other regular shapes of the same aggregate fraction. Fractal dimension and relative roughness are relatively more sensitive geometrical parameters to the effective diffusivity than other classical single-length parameters. At specific aggregate fraction, one promising prediction model for effective diffusivity can be proposed with only the two shape factors.

## Appendix 1: Derivation of $R_r$

As irregular aggregates are generated by the discrete Fast transformation, the roughness measured for a specific surface is based on the Parseval's formula of discrete Fast transformation:

$$\frac{1}{\pi}\int_0^{2\pi} l_0 + \sum_{n=1}^{N}\left[A_n\cos(n\theta) + B_n\sin(n\theta)\right]^2 d\theta = 2\left(l_0\right)^2 + \sum_{n=1}^{\infty} A_n^2 + \sum_{n=1}^{\infty} B_n^2. \tag{17}$$

Since $A_n{}^2 + B_n{}^2 = (F_n{}^2)(l_0{}^2)$, we arrive at

$$\frac{1}{\pi}\int_0^{2\pi} l_i\left(\theta_i\right)^2 d\theta = 2\left(l_0\right)^2 + \sum_{n=1}^{\infty}\left(F_n^2\right)\left(l_0^2\right) \tag{18}$$

Roughness is defined as the difference between generated irregular aggregate shape and $l_0$-determined circle, and thus, after the roughness is normalised by $l_0$-determined circle, the relative roughness is obtained as:

$$R_r = \frac{\sqrt{2\left(l_0\right)^2 + \sum_{n=1}^{\infty}\left(F_n^2\right)\left(l_0^2\right) - 2\left(l_0\right)^2}}{l_0}. \tag{19}$$

Considering $F_1 = 0$, $R_r$ can be expressed as:

$$R_r = \sqrt{\sum_{n=2}^{\infty}\left(F_n^2\right)} \tag{20}$$

Then, substitute $F_n = F_2\left(\frac{n}{2}\right)^{2F_d-4}$ in Sect. 2 into 20,

$$R_r = \sqrt{\sum_{n=2}^{\infty}\left(F_2^2\left(\frac{n}{2}\right)^{4F_d-8}\right)}, \tag{21}$$

## Appendix 2: Derivation of $HS_u$

According to the Hashin–Shrinkman (HS) variational theorems (Hashin and Shtrikman 1962), upper $D_{\text{eff,u}}$ and lower $D_{\text{eff,l}}$ bounds of 2D effective diffusivity for the two-phase composite are defined as (Torquato 1985):

$$D_{\text{eff,u}} = D_c\frac{1+\phi D_{a,c}}{1-\phi D_{a,c}}, \tag{22}$$

$$D_{\text{eff,l}} = D_a\frac{1+(1-\phi)D_{c,a}}{1-(1-\phi)D_{c,a}}, \tag{23}$$

where

$$D_{a,c} = \frac{D_a - D_c}{D_a + D_c} \quad \text{and} \quad D_{c,a} = \frac{D_c - D_a}{D_c + D_a} \tag{24}$$

Additionally, as aggregate phase in the diffusivity modelling assumes to be impermeable and $D_a = 0\text{m}^2/\text{s}$, $D_{\text{eff,u}}$ and $D_{\text{eff,l}}$ are divided by $(1-\phi)$ (Jiao and Torquato 2012; Liasneuski et al. 2014). Therefore, $D_{\text{eff,l}}$ is zero, and $D_{\text{eff,u}}$ becomes

$$D_{\text{eff,u}} = \frac{D_c}{1-\phi}\frac{1+\phi D_{a,c}}{1-\phi D_{a,c}} = \frac{D_c}{1+\phi}. \tag{25}$$

Dimensionless HS upper bounds ($HS_u$) of effective diffusivity can be finally defined as:

$$HS_u = \frac{D_{\text{eff,u}}}{D_c} = \frac{D_c}{(1+\phi)D_0}. \tag{26}$$

**Funding** No funding for this research work

## Declarations

**Conflict of interest** The authors declare that they have no conflict of interest.



## References

Abyaneh, S.D., Wong, H., Buenfeld, N.: Modelling the diffusivity of mortar and concrete using a three-dimensional mesostructure with several aggregate shapes. Comput. Mater. Sci. **78**, 63–73 (2013)

Bastidas-Arteaga, E., Chateauneuf, A., Sánchez-Silva, M., Bressolette, P., Schoefs, F.: A comprehensive probabilistic model of chloride ingress in unsaturated concrete. Eng. Struct. **33**(3), 720–730 (2011)

Caré, S.: Influence of aggregates on chloride diffusion coefficient into mortar. Cem. Concr. Res. **33**(7), 1021–1028 (2003)

Choy, T.C.: Effective medium theory: principles and applications, vol. 165. Oxford: Oxford University Press (2015)

Cui, G., Liu, M., Dai, W., Gan, Y.: Pore-scale modelling of gravity-driven drainage in disordered porous media. Int. J. Multiph. Flow **114**, 19–27 (2019)

Cui, W., Yan, W.-s., Song, H.-f., Wu, X.-l.: DEM simulation of SCC flow in L-Box set-up: Influence of coarse aggregate shape on SCC flowability. Cement Concrete Compos. **109**, 103558 (2020)

Delagrave, A., Marchand, J., Samson, E.: Prediction of diffusion coefficients in cement-based materials on the basis of migration experiments. Cem. Concr. Res. **26**(12), 1831–1842 (1996)

Denis, A., Attar, A., Breysse, D., Chauvin, J.J.: Effect of coarse aggregate on the workability of sandcrete. Cem. Concr. Res. **32**(5), 701–706 (2002)

Du, X., Jin, L., Ma, G.: A meso-scale numerical method for the simulation of chloride diffusivity in concrete. Finite Elem. Anal. Des. **85**, 87–100 (2014)

Erdoğan, S., Martys, N., Ferraris, C., Fowler, D.: Influence of the shape and roughness of inclusions on the rheological properties of a cementitious suspension. Cement Concr. Compos. **30**(5), 393–402 (2008)

Fantinel, P., Borgman, O., Holtzman, R., Goehring, L.: Drying in a microfluidic chip: experiments and simulations. Sci. Rep. **7**(1), 1–12 (2017)

Ferellec, J.-F., McDowell, G.J.G., Journal, G.A.I.: A simple method to create complex particle shapes for DEM. Geomech. Geoeng. **3**(3), 211–216 (2008)

Fernlund, J.M.R.: Image analysis method for determining 3-D shape of coarse aggregate. Cem. Concr. Res. **35**(8), 1629–1637 (2005)

Gjørv, O.E.: Durability of concrete structures. Arab. J. Sci. Eng. **36**(2), 151–172 (2011)

Guida, G., Viggiani, G.M., Casini, F.: Multi-scale morphological descriptors from the fractal analysis of particle contour. Acta Geotech. **15**(5), 1067–1080 (2020)

Hafid, H., Ovarlez, G., Toussaint, F., Jezequel, P., Roussel, N.: Effect of particle morphological parameters on sand grains packing properties and rheology of model mortars. Cem. Concr. Res. **80**, 44–51 (2016)

Hales, T.C.: The sphere packing problem. J. Comput. Appl. Math. **44**(1), 41–76 (1992)
Hashin, Z., Shtrikman, S.: A variational approach to the theory of the effective magnetic permeability of multiphase materials. J. Appl. Phys. **33**(10), 3125–3131 (1962)
Hoch, B.O.: Modelling of hydrogen diffusion in heterogeneous materials: implications of the grain boundary connectivity. Université de La Rochelle (2015)
Holtzman, R.: Effects of pore-scale disorder on fluid displacement in partially-wettable porous media. Sci. Rep. **6**, 36221 (2016)
Hornung, U.: Homogenization and porous media, vol. 6. Cham, Springer Science & Business Media (1996)
Idiart, A.E., López, C.M., Carol, I.: Chemo-mechanical analysis of concrete cracking and degradation due to external sulfate attack: A meso-scale model. Cement Concr. Compos. **33**(3), 411–423 (2011)
Jiao, Y., Torquato, S.: Quantitative characterization of the microstructure and transport properties of biopolymer networks. Phys. Biol. **9**(3), 036009 (2012)
Jie, W., Dassekpo, J.-B.M., Wan, C., Zha, X.: Experimental and numerical modeling of chloride diffusivity in hardened cement concrete considering the aggregate shapes and exposure-duration effects. Results in Physics **7**, 1427–1432 (2017)
Jóhannesson, H., Halle, B.: Solvent diffusion in ordered macrofluids: a stochastic simulation study of the obstruction effect. J. Chem. Phys. **104**(17), 6807–6817 (1996)
Krejsová, J., Doleželová, M., Pernicová, R., Svora, P., Vimmrová, A.: The influence of different aggregates on the behavior and properties of gypsum mortars. Cement Concr. Compos. **92**, 188–197 (2018)
Kwan, A.K., Mora, C., Chan, H.: Particle shape analysis of coarse aggregate using digital image processing. Cem. Concr. Res. **29**(9), 1403–1410 (1999)
Laubie, H., Monfared, S., Radjai, F., Pellenq, R., Ulm, F.-J.: Disorder-induced stiffness degradation of highly disordered porous materials. J. Mech. Phys. Solids **106**, 207–228 (2017a)
Laubie, H., Radjai, F., Pellenq, R., Ulm, F.-J.: Stress transmission and failure in disordered porous media. Phys. Rev. Lett. **119**(7), 075501 (2017b)
Li, L.-Y., Xia, J., Lin, S.-S.: A multi-phase model for predicting the effective diffusion coefficient of chlorides in concrete. Constr. Build. Mater. **26**(1), 295–301 (2012)
Liasneuski, H., Hlushkou, D., Khirevich, S., Höltzel, A., Tallarek, U., Torquato, S.: Impact of microstructure on the effective diffusivity in random packings of hard spheres. J. Appl. Phys. **116**(3), 034904 (2014)
Liu, L., Sun, W., Ye, G., Chen, H., Qian, Z.: Estimation of the ionic diffusivity of virtual cement paste by random walk algorithm. Constr. Build. Mater. **28**(1), 405–413 (2012)
Liu, L., Shen, D., Chen, H., Xu, W.: Aggregate shape effect on the diffusivity of mortar: a 3D numerical investigation by random packing models of ellipsoidal particles and of convex polyhedral particles. Comput. Struct. **144**, 40–51 (2014)
Liu, C., Xie, D., She, W., Liu, Z., Liu, G., Yang, L., Zhang, Y.: Numerical modelling of elastic modulus and diffusion coefficient of concrete as a three-phase composite material. Constr. Build. Mater. **189**, 1251–1263 (2018)
Luping, T., Gulikers, J.: On the mathematics of time-dependent apparent chloride diffusion coefficient in concrete. Cem. Concr. Res. **37**(4), 589–595 (2007)
Luping, T., Nilsson, L.-O.: Rapid determination of the chloride diffusivity in concrete by applying an electric field. Mater. J. **89**(1), 49–53 (1993)
Ma, H., Xu, W., Li, Y.: Random aggregate model for mesoscopic structures and mechanical analysis of fully-graded concrete. Comput. Struct. **177**, 103–113 (2016)
MacDonald, K.A., Northwood, D.O.: Experimental measurements of chloride ion diffusion rates using a two-compartment diffusion cell: Effects of material and test variables. Cem. Concr. Res. **25**(7), 1407–1416 (1995)
Mollon, G., Zhao, J.: Fourier–Voronoi-based generation of realistic samples for discrete modelling of granular materials. Granular Matter **14**(5), 621–638 (2012)
Mora, C., Kwan, A.: Sphericity, shape factor, and convexity measurement of coarse aggregate for concrete using digital image processing. Cem. Concr. Res. **30**(3), 351–358 (2000)
Pae, J., Zhang, Y., Poh, L.H., Moon, J.: Three-dimensional transport properties of mortar with a high water-to-cement ratio using X-ray computed tomography. Constr. Build. Mater. **281**, 122608 (2021)
Page, C., Short, N., El Tarras, A.: Diffusion of chloride ions in hardened cement pastes. Cem. Concr. Res. **11**(3), 395–406 (1981)
Page, C., Ngala, V., Parrot, L., Yu, S.: Diffusion in cementitious materials: further investigations of chloride and oxygen diffusion in well-cured opc and opc/30% PFA pastes. Cem. Concr. Res **25**(4), 819–826 (1995)
Pan, Z., Chen, A., Ruan, X.: Spatial variability of chloride and its influence on thickness of concrete cover: A two-dimensional mesoscopic numerical research. Eng. Struct. **95**, 154–169 (2015)

Patel, R.A., Phung, Q.T., Seetharam, S.C., Perko, J., Jacques, D., Maes, N., De Schutter, G., Ye, G., Van Breugel, K.: Diffusivity of saturated ordinary Portland cement-based materials: A critical review of experimental and analytical modelling approaches. Cem. Concr. Res. **90**, 52–72 (2016)

Pivonka, P., Hellmich, C., Smith, D.: Microscopic effects on chloride diffusivity of cement pastes—a scale-transition analysis. Cem. Concr. Res. **34**(12), 2251–2260 (2004)

Pollmann, N., Larsson, F., Runesson, K., Lundgren, K., Zandi, K., Jänicke, R.: Modeling and computational homogenization of chloride diffusion in three-phase meso-scale concrete. Constr. Build. Mater. **271**, 121558 (2021)

Rocco, C., Elices, M.: Effect of aggregate shape on the mechanical properties of a simple concrete. Eng. Fract. Mech. **76**(2), 286–298 (2009)

Ruan, X., Li, Y., Jin, Z., Pan, Z., Yin, Z.: Modeling method of concrete material at mesoscale with refined aggregate shapes based on image recognition. Constr. Build. Mater. **204**, 562–575 (2019)

Santos, A.R., do Rosário Veiga, M., Silva, A.S., de Brito, J.: Microstructure as a critical factor of cement mortars' behaviour: The effect of aggregates' properties. Cement Concrete Compos. 103628 (2020)

Savvas, D., Stefanou, G., Papadrakakis, M.: Determination of RVE size for random composites with local volume fraction variation. Comput. Methods Appl. Mech. Eng. **305**, 340–358 (2016)

Shafikhani, M., Chidiac, S.: Quantification of concrete chloride diffusion coefficient—a critical review. Cement Concr. Compos. **99**, 225–250 (2019)

Sun, G., Zhang, Y., Sun, W., Liu, Z., Wang, C.: Multi-scale prediction of the effective chloride diffusion coefficient of concrete. Constr. Build. Mater. **25**(10), 3820–3831 (2011)

Torquato, S.: Effective electrical conductivity of two-phase disordered composite media. J. Appl. Phys. **58**(10), 3790–3797 (1985)

Torquato, S., Haslach, H., Jr.: Random heterogeneous materials: microstructure and macroscopic properties. Appl. Mech. Rev. **55**(4), B62–B63 (2002)

Ueno, A., Ogawa, Y.: Influence of coarse aggregate shape on optimum fine to total aggregate ratio using a virtual voids-ratio diagram in concrete compaction. Cement Concr. Compos. **106**, 103463 (2020)

Wadell, H.J.T.J.o.G.: Volume, shape, and roundness of rock particles. **40**(5), 443–451 (1932)

Wang, X., Liang, Z., Nie, Z., Gong, J.: Stochastic numerical model of stone-based materials with realistic stone-inclusion features. Constr. Build. Mater. **197**, 830–848 (2019a)

Wang, Z., Chauhan, K., Pereira, J.-M., Gan, Y.: Disorder characterization of porous media and its effect on fluid displacement. Phys. Rev. Fluids **4**(3), 034305 (2019b)

Wei, D., Wang, J., Nie, J., Zhou, B.: Generation of realistic sand particles with fractal nature using an improved spherical harmonic analysis. Comput. Geotech. **104**, 1–12 (2018)

Wei, D., Hurley, R.C., Poh, L.H., Dias-da-Costa, D., Gan, Y.: The role of particle morphology on concrete fracture behaviour: a meso-scale modelling approach. Cem. Concr. Res. **134**, 106096 (2020)

Westerholm, M., Lagerblad, B., Silfwerbrand, J., Forssberg, E.: Influence of fine aggregate characteristics on the rheological properties of mortars. Cement Concr. Compos. **30**(4), 274–282 (2008)

Xiao, J., Ying, J., Shen, L.: FEM simulation of chloride diffusion in modeled recycled aggregate concrete. Constr. Build. Mater. **29**, 12–23 (2012)

Xiong, Q., Wang, X., Jivkov, A.P.: A 3D multi-phase meso-scale model for modelling coupling of damage and transport properties in concrete. Cement Concr. Compos. **109**, 103545 (2020)

Xu, J., Li, F.: A meso-scale model for analyzing the chloride diffusion of concrete subjected to external stress. Constr. Build. Mater. **130**, 11–21 (2017)

Xu, W., Xu, B., Guo, F.: Elastic properties of particle-reinforced composites containing nonspherical particles of high packing density and interphase: DEM–FEM simulation and micromechanical theory. Comput. Methods Appl. Mech. Eng. **326**, 122–143 (2017)

Yu, S., Page, C.: Diffusion in cementitious materials: 1. Comparative study of chloride and oxygen diffusion in hydrated cement pastes. Cement Concrete Res. **21**(4), 581–588 (1991)

Zhang, M., Ye, G., van Breugel, K.: Modeling of ionic diffusivity in non-saturated cement-based materials using lattice Boltzmann method. Cem. Concr. Res. **42**(11), 1524–1533 (2012)

Zhang, Z., Song, X., Liu, Y., Wu, D., Song, C.: Three-dimensional mesoscale modelling of concrete composites by using random walking algorithm. Compos. Sci. Technol. **149**, 235–245 (2017)

Zhang, M., Ye, G., van Breugel, K.: Multiscale lattice Boltzmann-finite element modelling of chloride diffusivity in cementitious materials. Part I: Algorithms and implementation. Mechanics Research Communications **58**, 53–63 (2014)

Zhang, M.: Multiscale lattice Boltzmann-finite element modelling of transport properties in cement-based materials. Thesis (PhD) Delft University of Technology (2013)

Zheng, J., Hryciw, R.D.: Traditional soil particle sphericity, roundness and surface roughness by computational geometry. Géotechnique **65**(6), 494–506 (2015)

Zheng, J.-J., Zhou, X.-Z., Wu, Y.-F., Jin, X.-Y.: A numerical method for the chloride diffusivity in concrete with aggregate shape effect. Constr. Build. Mater. **31**, 151–156 (2012)
Zheng, J., Zhang, C., Wu, Y., Sun, L.: Random-walk algorithm for chloride diffusivity of concrete with aggregate shape effect. J. Mater. Civ. Eng. **28**(12), 04016153 (2016)
Zhou, C., Li, K., Ma, F.: Numerical and statistical analysis of elastic modulus of concrete as a three-phase heterogeneous composite. Comput. Struct. **139**, 33–42 (2014)



## Authors and Affiliations

**Qingchen Liu[1] · Deheng Wei[1] · Hongzhi Zhang[2] · Chongpu Zhai[4] · Yixiang Gan[1,3]**

[1] School of Civil Engineering, The University of Sydney, Sydney, NSW 2006, Australia

[2] School of Transportation, Shandong University, Jinan, Shandong Province, People's Republic of China

[3] The University of Sydney Nano Institute (Sydney Nano), The University of Sydney, Sydney, NSW 2006, Australia

[4] State Key Laboratory for Strength and Vibration of Mechanical Structures, School of Aerospace, Xi'an Jiaotong University, Xi'an 710049, China